Electro-mechanical impedance (EMI)-based incipient crack monitoring and critical crack identification of beam structures

Lim, Yee Yan; Soh, Chee Kiong

2014

Lim, Y. Y., & Soh, C. K. (2014). Electro-mechanical impedance (EMI)-based incipient crack monitoring and critical crack identification of beam structures. Research in nondestructive evaluation, 25(2), 82-98.

https://hdl.handle.net/10356/106648

https://doi.org/10.1080/09349847.2013.848311

Research in Nondestructive Evaluation
Publication details, including instructions for authors and subscription information:
http://www.tandfonline.com/loi/urnd20

Electro-Mechanical Impedance (EMI)-Based Incipient Crack Monitoring and Critical Crack Identification of Beam Structures

Yee Yan Lim [a] & Chee Kiong Soh [b]

[a] Civil Engineering Program, School of Environment , Science and Engineering, Southern Cross University , Lismore , Australia

[b] Division of Structures and Mechanics, School of Civil and Environmental Engineering , Nanyang Technological University , Singapore

Accepted author version posted online: 13 Nov 2013.Published online: 09 May 2014.

To cite this article: Yee Yan Lim & Chee Kiong Soh (2014) Electro-Mechanical Impedance (EMI)-Based Incipient Crack Monitoring and Critical Crack Identification of Beam Structures, Research in Nondestructive Evaluation, 25:2, 82-98, DOI: 10.1080/09349847.2013.848311

To link to this article: http://dx.doi.org/10.1080/09349847.2013.848311

Research in Nondestructive Evaluation, 25:82–98, 2014

ISSN: 0934-9847 print/1432-2110 online
DOI: 10.1080/09349847.2013.848311

Taylor & Francis
Taylor & Francis Group

ELECTRO-MECHANICAL IMPEDANCE (EMI)-BASED INCIPIENT CRACK MONITORING AND CRITICAL CRACK IDENTIFICATION OF BEAM STRUCTURES

Yee Yan Lim[1] and Chee Kiong Soh[2]

[1]Civil Engineering Program, School of Environment, Science and Engineering, Southern Cross University, Lismore, Australia
[2]Division of Structures and Mechanics, School of Civil and Environmental Engineering, Nanyang Technological University, Singapore

Fatigue-induced damage is often progressive and gradual in nature. Fatigue is often deteriorated by corrosion in ageing structures, creating maintenance problems, and even causing catastrophic failure. This ushers the development of structural health monitoring (SHM) and nondestructive evaluation (NDE) systems. Recent advent of smart materials applicable in SHM alleviates the shortcomings of the conventional techniques. Autonomous, real-time, remote monitoring becomes possible with the use of smart piezoelectric transducers. For instance, the electro-mechanical impedance (EMI) technique, employing piezoelectric transducers as collocated actuators and sensors, is known for its ability in damage detection and characterization. This article presents a series of lab-scale experimental tests and analysis to investigate the feasibility of fatigue crack detection and characterization employing the EMI technique. This study extends the work by Lim and Soh [1] to incorporate the phases involving crack initiation and critical crack. It is suggested that the EMI technique is effective in characterizing fatigue induced cracking, even in its incipient stage. Micro-crack invisible to the naked eyes can be detected by the technique especially when employing the higher frequency range of 100–200 kHz. A quick and handy qualitative-based critical crack identification method is also suggested by visually inspecting the admittance frequency spectrum.

Keywords: electromechanical impedance (EMI) technique, fatigue, micro-crack, piezoelectric materials, structural health monitoring (SHM)

1. INTRODUCTION

Structures and structural components in service are often subjected to repeated fluctuating stresses, often known as fatigue loading, of magnitude lower than that of their strength limit. Fatigue induced damage

Address correspondence to Yee Yan Lim, Civil Engineering Program, School of Environment, Science and Engineering, Southern Cross University, Lismore, NSW 2480, Australia. E-mail: limy0134@ntu.edu.sg

Color versions of one or more of the figures in the article can be found online at www.tandfonline.com/urnd.

is often progressive and gradual in nature. Structures subjected to large number of fatigue load cycles will progressively encounter three phases, namely the process of crack initiation, crack propagation, and critical crack. Upon reaching the critical crack, it would propagate rapidly rendering the structure to fail in a fracture manner. This type of failure is often known as fatigue failure. Fuchs and Stephens [2] reported that up to 90% of structural failures are caused by fatigue.

In the conventional structural design, conservative estimation of fatigue life is adopted to ensure safety. However, it is often noticed that the structure or structural member remains functional despite their design life being reached. On the other hand, premature failure could occur when the actual loading exceeds the estimated loading significantly. Therefore, it is of general interest to develop a reliable technique which could accurately identify the status of the structure in service and thus predict the remaining life of the structure.

In practice, it is essential to develop a technique capable of detecting crack at the earliest possible stage of the process. On the other hand, it should also be capable of characterizing the crack and estimating the remaining useful life of the structure. In terms of metal fatigue, the non-destructive testing (NDT) is expected to detect the presence of crack as well as to measure its size. Some of the commonly used NDT techniques include visual inspection, magnetic particle inspection, radiography, ultrasonic, and electromagnetic fields [3]. Although some of these techniques are effective in sizing fatigue cracks and have been well established, major drawbacks exist such as the location of crack has to be known *a priori*, difficulty in automation, interruption of service, disassembly of device, as well as cost and labor intensive.

Recently, the emergence of smart material based sensing such as using the electro-mechanical impedance (EMI) technique could possibly provide an alternative to the conventional techniques, overcoming some of the major drawbacks. The EMI technique, employing piezoelectric or PZT (lead zirconate titanate) transducer as collocated actuator and sensor is potentially applicable in this aspect with its widely known capability to detect and characterize damage. It offers advantages such as autonomous, real-time, and remote monitoring. The installation of PZT transducers is normally non-intrusive to the structure, and the transducers are capable of detecting various damages [4]. In addition, piezoelectric materials are also frequently used as passive dampers [5,6] and energy harvesters [7].

Most of the previous studies on fatigue crack monitoring using the EMI technique focus on the crack propagation process. The sensitivity of the EMI technique towards micro-crack in the crack initiation process and the method for detecting critical crack are scarcely available.

This study extends the work by Lim and Soh [1], where a semi-analytical damage prognosis model useful for estimating the remaining life of 1-D beam was proposed. The model considers implicitly all three

phases (crack initiation, crack propagation, and critical crack) of fatigue crack. No special attention was paid to the phases of crack initiation and critical crack. In this article, the feasibility of employing the EMI technique to detect micro-crack invisible to the naked eyes is investigated, and the sensitivity of different frequency ranges is analyzed. A qualitative-based critical crack identification method is also proposed. In a nutshell, the damage prognosis model developed by Lim and Soh is further strengthened by the additional methods recommended in this study.

2. PHYSICAL PRINCIPLES OF EMI TECHNIQUE

Sun et al. [8] first proposed the use of PZT transducers to monitor structural health by utilizing their ability to convert electrical energy into mechanical energy and vice versa. With the PZT transducer affixed to the host structure, an alternating voltage of varying frequency is applied by an impedance analyzer across the poling direction of the transducer. The transducer can thus be excited (converse effect of piezoelectricity) and correspondingly actuates the host structure. On the other hand, the structural response interacts with the PZT transducer, thus modulating the current passing through the transducer (direct effect of piezoelectricity). The modulated current, in terms of complex electrical admittance or impedance, can simultaneously be measured by the impedance analyzer. In other words, the admittance signatures contain information pertinent to the modes of vibration of the host structure. Any changes in the vibrational behavior of the host structure caused by degradation, disintegration, damage, etc., would therefore be reflected in the admittance signatures.

A theoretical model for the dynamics of PZT-structure interaction was proposed by Giurgiutiu and Zagrai [9] using an elastically constrained boundary condition represented by a pair of springs (dynamic stiffness, K_{str}) at both ends of the PZT patch as shown in Fig. 1. The drive point dynamic stiffness represents the host structure's interaction with the PZT patch at its end points. This approach of modeling allows for a complete range of transducer boundary condition to be investigated. The complex electrical admittance, Y, can be expressed as

$$Y = j\omega C\left[1 - \kappa_{31}^2\left(1 - \frac{1}{\theta\cot(\theta) + R}\right)\right], \tag{1}$$

where $\theta = \frac{\gamma l_a}{2}$, and $C = l_a b_a \bar{\varepsilon}_{33}^T h_a^{-1}$ is the zero load capacitance. l_a, b_a, and h_a are the length, width, and thickness of the transducer, respectively. γ is the wave number, ω is the angular frequency, and j denotes imaginary number. $R = K_{str}/K_{PZT}$ is the stiffness ratio between host structure and PZT patch, and $K_{PZT} = A_a \bar{Y}_{11}^E / l_a$ and A_a are the quasi-static stiffness and the cross-sectional area of the patch, respectively. $\bar{\varepsilon}_{33}^T$ and $\bar{Y}_{11}^E$ are the complex

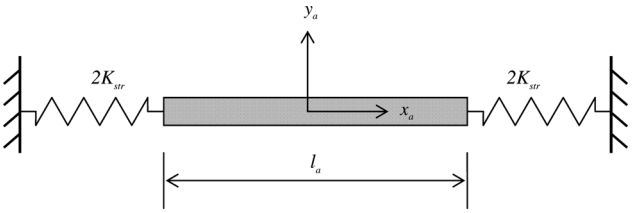

FIGURE 1. Elastically constrained 1-D PZT-structure interaction model. © SAGE Publications. Reproduced by permission of SAGE Publications. Permission to reuse must be obtained from the rightsholder.

electrical permittivity and complex Young's modulus of transducer. $\kappa_{31} = \sqrt{\frac{d_{31}^2 \bar{Y}_{11}^E}{\bar{\varepsilon}_{33}^T}}$ is the EM cross-coupling coefficient of the PZT patch, and d_{31} is the piezoelectric strain coefficient.

Essentially, the EMI technique shares similar working principles as the conventional global dynamic response techniques, but the frequency range employed in the EMI technique (30–1,000 kHz) is much higher. The use of high frequency of excitation renders the EMI technique to be very effective in detecting local damage, even in its incipient stage. Naidu and Bhalla [10] showed the robustness of the EMI technique in characterizing damages induced in concrete structure. Giurgiutiu [11] performed experimental test to monitor the debonding of FRP composite reinforcing strips surface mounted on concrete beam during a fatigue test. The PZT patch's resonance was selected as indication of damage, whereby the peak's amplitude gradually increased upon debonding. Lim et al. [12] presented some parametric-based damage detection using equivalent structural parameters in characterizing the severity of damage in a structure. Park et al. [13] adopted the principal component analysis data (PCA-data) compression technique as a preprocessing module to reduce the data dimensionality and eliminate the unwanted noises. Lim and Soh [14,15] presented a series of investigative studies on the effects of boundary condition and axial load on the admittance signatures acquired from the EMI technique.

The EMI technique also shows its ability in monitoring the hydration process of concrete. For instance, Shin et al. [16] showed that the EMI signatures obtained from PZT patch surface bonded on concrete gradually shift to the right and subside with curing time. They concluded that these behaviors are attributed to stiffening action caused by strength gain of concrete. Yang et al. [17] proposed a reusable PZT transducer setup for simultaneous monitoring of concrete hydration as well as structural health.

Comprehensive reviews on the EMI technique can be found in [4,18,19].

3. FATIGUE CRACK DETECTION AND CHARACTERIZATION USING PZT TRANSDUCERS

Giurgiutiu et al. [20] performed incremental damage tests of spot-welded lap-joint shear specimen under fatigue loading. The root mean square deviation (RMSD) index of impedance signatures in the frequency range of 200–1,100 kHz was correlated with the stiffness loss, which in turn quantified the structural damage. The stiffness-damage correlation principle was used to quantify progression of damage and estimation of fatigue life.

Giurgiutiu et al. [21] showed that the EMI technique and the Lamb-wave technique applied with piezoelectric wafer active sensor are both able to detect the presence and propagation of a crack under mixed-mode fatigue loading. They observed that some PZT patches disbonded from the specimen after the test, which could be caused by plasticity effect near the crack tip. Thus, they suggested that the placing of transducers should avoid the highly strained areas.

Sovostianov et al. [22] conducted experimental investigation on the relationship between strength reduction caused by accumulated damage in elastic electrically conductive material, its corresponding electrical resistance across the damaged specimen and the EMI response. The structural impedance peak was found to decrease steadily in peak frequency over the number of loading cycles.

Kim [23] demonstrated the effectiveness of EMI technique in monitoring welded structural members while in service. He also adopted one PZT transducer as sensor and another as actuator. He found that the measurement that crossed the crack path produced increase in damage metric. Fiber Bragg Grating sensor was also attached for stress measurement, and this integrated technique was found to provide ideal characteristics for detecting damage on structure in service.

Ihn and Chang [24] employed the wave propagation technique using built-in PZT patches for damage detection. Structural damage was detected from changes in the received signal. They proved that the technique is effective in detecting debonding or delamination as well as in monitoring fatigue crack growth [25].

Soh and Lim [26] investigated the feasibility of fatigue induced damage detection and characterization using the EMI technique. Experimental study on an aluminum beam with a pre-induced circular notch indicated that the EMI technique is excellent in detecting fatigue crack through changes in admittance signature's frequency.

Some other researchers [27,28] also conducted study using statistical quantifiers to characterize fatigue crack propagation.

4. FATIGUE CRACK GROWTH

Subcritical crack could grow under fatigue load until a critical size is reached. Once the critical crack is reached, failure is impending. Relationship between different fatigue crack growth rates is conveniently related to the applied stress intensity factor range, as shown in Fig. 2, in log scale which can generally be divided into 3 regions. Region I is the threshold region as indicated by a threshold value, ΔKth, below which fatigue cracks are characterized as nonpropagating.

Region II, commonly known as Paris region, depicts an essentially linear relationship between crack growth rate, da/dN, and stress intensity factor range, ΔK, in logarithmic scale. In typical engineering design, region II is often adopted as it covers the largest range of intensity.

In region III, the fatigue crack growth rate is very high resulting in unstable propagation. Although the plastic zone size is often big in this region, it is normally neglected because very little fatigue life is involved in this region as fracture failure is fast approaching. In real-life design, extrapolation of region II into both regions I and III are often acceptable as it provides conservative fatigue life prediction.

In actual application, if the stress intensity factor range is known, the fatigue life of the component can be obtained by integrating the sigmoidal curve between the limits of the initial crack size and final crack size. For instance within the Paris region, the number of cycles to failure, N, for a rectangular aluminum beam with a single edge crack loaded in tension can be expressed as [29]

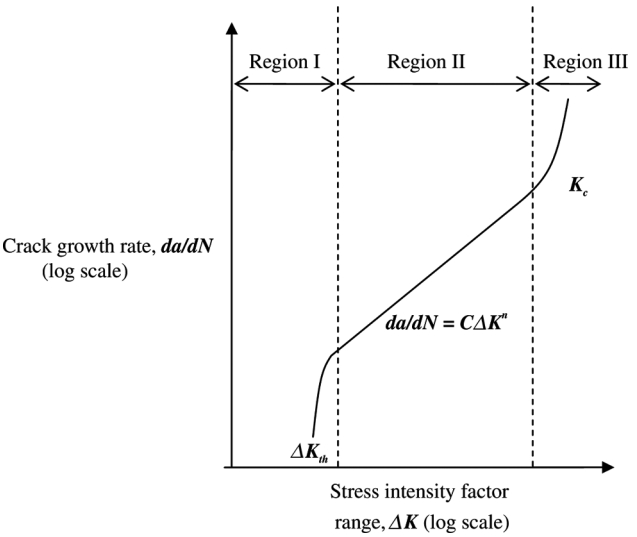

FIGURE 2. Schematic sigmoidal behavior of typical fatigue crack growth rate versus stress intensity factor range of metal.

$$N = \frac{1}{C'(\Delta\sigma)^m} \int_{a0}^{af} \frac{da}{\left[1.99a^{1/2} - 0.41\frac{a^{3/2}}{w} + 18.7\frac{a}{w^2}^{5/2} - 38.48\frac{a}{w^3}^{7/2} + 53.85\frac{a}{w^4}^{9/2}\right]^m} \quad (2)$$

in which C' and m are material dependent constants, $\Delta\sigma$ is the stress range, w is the beam width, a is the crack length, and a_0 and a_f are the initial and final crack length, respectively.

5. FATIGUE CRACK CHARACTERIZATION USING EMI TECHNIQUE

5.1. Experimental Setup and Procedures

Experimental tests were conducted following similar procedures as adopted in Lim and Soh [1]. Three identical lab-sized aluminium beams (T6061-T6) were prepared. The dimensions of the beam were 300 mm × 50 mm × 6 mm. The specimens were labeled as S1, S2, and S3, respectively.

One piece of PZT patch dimensioned 10 mm × 10 mm × 0.3 mm, manufactured by PI Ceramic [30], was surface-bonded on each of the specimens (located at one-quarter of the specimen's length from one end) using two parts high strength epoxy as shown in Fig. 3. The PZT patches used in this study were PIC 151, a modified lead zirconate titanate ceramic with high permittivity, high coupling factor, and high charge constant. A layer of silicone rubber was coated above the PZT patch to protect it against wear and tear during specimen preparation and testing [31].

For each of the specimens, an initial single edge crack (measured 4.75 mm) was created at the center of the specimen using electric discharge machining (EDM) to serve as stress concentration. Under mode I loading, fatigue crack is expected to initiate at the tip of the edge notch and propagate perpendicularly to the direction of loading. All specimens were successfully tested to failure.

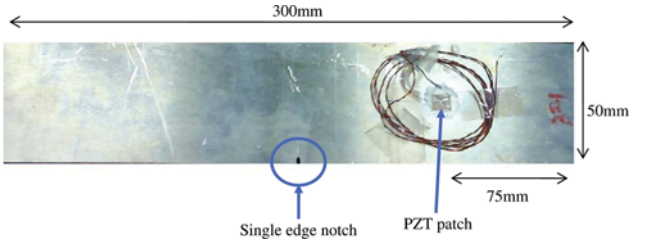

FIGURE 3. Aluminum beam specimen with single edge notch and a piece of PZT patch surface-bonded at one-quarter length from one end.

Uniaxial cyclic tensile load was applied to the specimen using a 25 ton dynamic testing machine (Fig. 4(a)) at predetermined intervals to induce mode I (opening mode) constant stress amplitude fatigue load. Nominal stress applied was controlled between 40–50% of the yield stress of the aluminium beam, which asserted a mean stress of 134.6 MPa and an alternating stress of 15.0 MPa.

Wayne Kerr precision impedance analyzer 6420 (Fig. 4(b)) was used to supply the alternating voltage and to measure the corresponding admittance signatures in the application of the EMI technique. A notebook

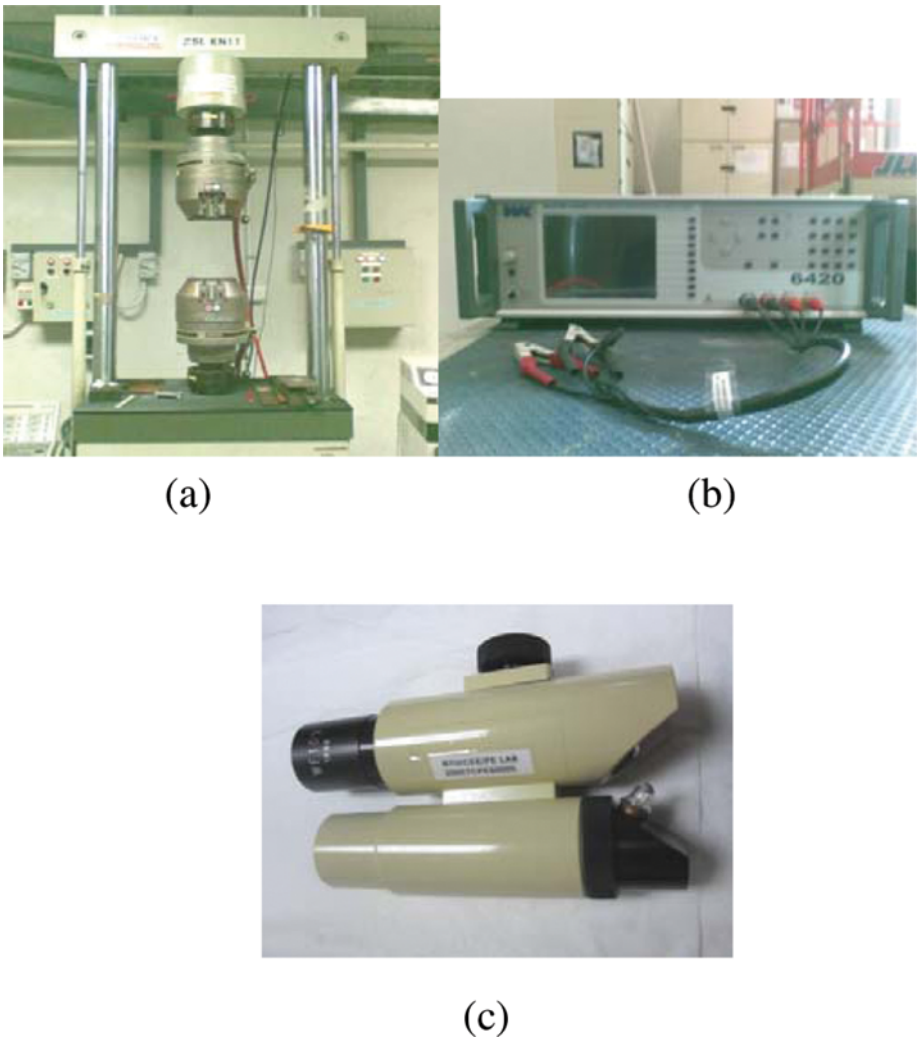

FIGURE 4. (a) 25 ton dynamic testing machine; (b) precision impedance analyzer; (c) crack detector.

TABLE 1 Summary of crack length at various number of cycles for aluminium beam specimens

Specimens	No. of cycles to first observable crack (0.2 mm)	No. of cycles to first visible crack (1 mm)	No. of cycles to failure	Critical crack length
S1	120,000	160,000	240,000	18 mm
S2	120,000	160,000	225,000	17 mm
S3	100,000	160,000	220,000	17 mm

computer with customized software was used to record the admittance signatures. A crack detector of 0.02 mm resolution was used for measuring the crack length as shown in Fig. 4(c).

Baseline admittance signatures of the PZT patch surface-bonded on the beam specimen was first recorded at healthy stage (before application of load) in the frequency range of 10–200 kHz. Cyclic tensile load was then applied at stages with predetermined number of cycles. The specimen was removed from the machine after each stage for the acquisition of admittance signatures in free-ended condition to prevent contamination caused by the effect of clamping and loading [14,15]. Initiation and propagation of crack from the edge notch was closely monitored using the crack detector.

The specimen was loaded in stages up to failure. The other specimens were similarly tested. The number of cycles at crack initiation, first crack, critical crack, and failure were recorded. It should be noted that the specimens failed shortly (generally less than 1,000 cycles) after reaching their critical crack length. The critical crack lengths as well as the number of cycles to failure are summarized in Table 1. Kindly note that the values are rounded to the nearest 1000. In this study, first crack is defined as a 1 mm crack, which occurred at approximately 160,000 cycles for all specimens. Thus, the period before 160,000 cycles is considered as the crack initiation process whereas the period after 160,000 cycles is the crack propagation process. All PZT patches remained functional after failure of the host structures.

5.2. Resonance Peaks from Conductance Signatures as Damage Quantifier

As suggested by Lim and Soh [1], damage characterization can be achieved by quantifying the movement of structural resonance peaks in the admittance signatures spectrum. The resonance peaks represent the dynamic behavior of the host structure. In this study, conductance (real component of admittance) signatures are used as damage quantifier due to its higher sensitivity towards damage than its imaginary counterpart [5]. Frequency range adopted is from 10–200 kHz. The advantages of different frequency ranges will be discussed.

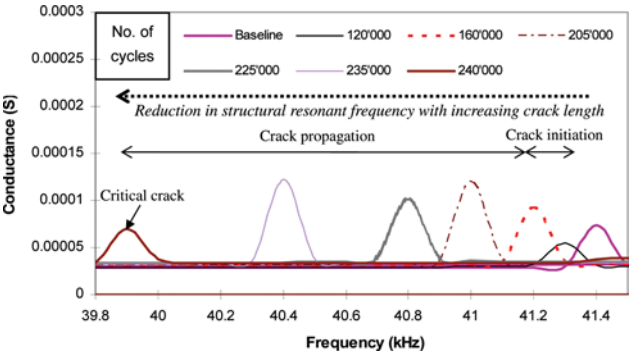

FIGURE 5. Conductance signatures versus frequency (39.8 ~ 41.5 kHz) acquired from PZT patch surface-bonded on specimen S1 after different number of loading cycles.

Figure 5 plots a selected structural resonance peak of specimen S1, recorded at different health conditions, 0 cycle (baseline) to 240,000 cycles (critical crack). The peak of baseline signature occurs at 41.4 kHz. Gradual and progressive horizontal leftward movements of the resonance peak at different loading stages can be observed. The result from this section has been reported in Lim and Soh [1], which will only be briefly discussed.

The shift in resonance peak could reflect the severity of cracking encountered by the specimen. Leftward movements of the first 3 peaks (baseline, 120,000 cycles, and 160,000 cycles) are minimal (0.2 kHz) indicating only mild structural damage is inflicted. Referring to the physical condition of the specimen, first crack (1.3 mm) is observed after 160,000 cycles. Therefore, the crack remained predominantly in its microscopic level below 160,000 cycles. We could infer that the specimen is undergoing the process of crack initiation, which consisted of up to 70% of its total life. Above 160,000 cycles, the rate of movement of peaks increases significantly denoting higher rate of crack propagation.

Upon loading to 240,000 cycles, which indicated the occurrence of critical crack, a sudden reduction in 0.5 kHz of its resonance frequency is observed, implying that very serious damage has been inflicted.

It is worth mentioning that the leftward movement of peak is caused by a reduction in resonance frequency, which is in line with the structural dynamic theory whereby an increase in damage severity reduces the stiffness of the structure, which can be reflected from the leftward motion of the structural resonance peak.

5.3. Monitoring Crack Initiation Process (Phase I)

Figure 6 shows two diagrams illustrating selected resonance peaks in two different frequency ranges acquired on specimen S2 from 0

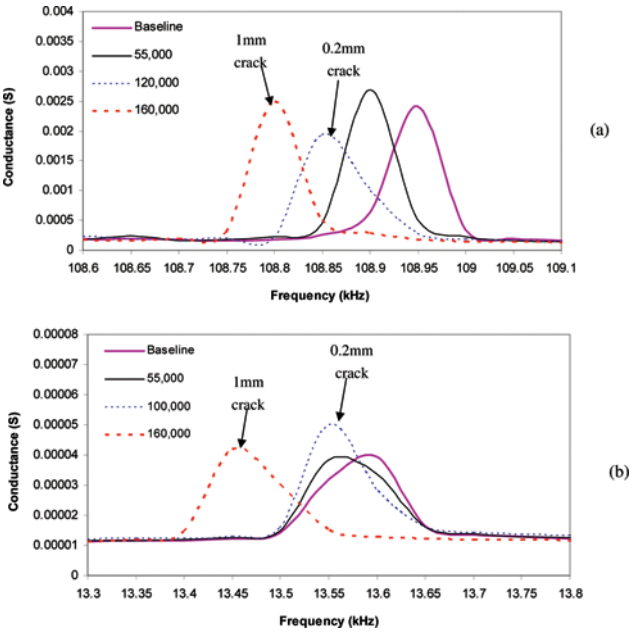

FIGURE 6. Conductance signatures acquired from PZT patch surface bonded on specimen S2 subjected to cyclic load from 0 to 160, 000 cycles. (a) 108.6 to 109.1 kHz; (b) 13.3 to 13.8 kHz.

cycle (baseline) to 160,000 cycles (occurrence of first crack). This figure illustrates the peaks acquired predominantly in the crack initiation process. First crack (1 mm) occurs at 160,000 cycles, while a 0.2 mm surface crack occurs at 120,000 cycles.

Figure 6(a) shows a series of peak occurring at about 109 kHz. The leftward movement of resonance peak is very sensitive to fatigue induced crack, even in its initiation period. A 0.2 mm crack detected using the crack detector after 120,000 cycles is invisible to the naked eye. Incipient crack at 55,000 cycles is even undetectable using the crack detector, but both could be effectively picked up by the EMI technique.

However, it should also be noted that the sensitivity shown in Fig. 6(a) becomes much lower when the lower frequency range is adopted, as shown in Fig. 5(b). Using the 10 to 20 kHz range, the detection of first crack (160,000 cycles) remains feasible but the detection of micro-crack appears to be less effective, as reflected from the near overlapping of the first three peaks.

To further understand the sensitivity of EMI technique towards micro-crack, more resonance peaks are investigated throughout the frequency spectrum. Approximately four major resonance peaks within 20 kHz range are selected and their sensitivity analyzed by calculating the reduction in resonance frequency per millimeter increase in crack length. The

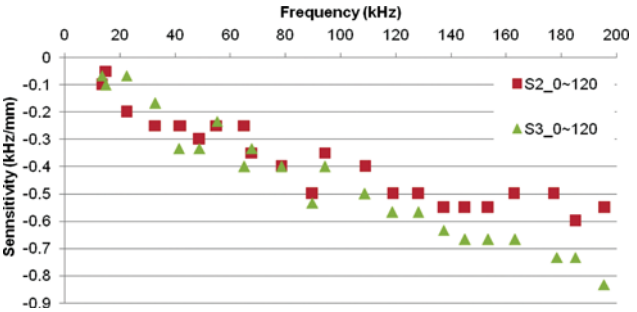

FIGURE 7. Sensitivity of structural resonance peaks towards micro-crack (≤ 0.2 mm) throughout the frequency spectrum ($10 \sim 200$ kHz).

calculation is based on the reduction in frequency for crack at 0.2 mm in comparison to the healthy stage. The outcome is summarized in Fig. 7.

This figure further supports the premise that sensitivity increases with frequency and higher frequency range is more sensitive to micro-crack. Sensitivity of EMI technique in the 200 kHz range is approximately 7 to 8 times higher than those in the 20 kHz range.

This phenomenon can be readily explained by looking at the fundamentals of the EMI technique. In this technique, standing wave is activated by PZT patch to the host structure which induces a forced harmonic vibration. When a damage such as a crack is induced, the standing wave is interfered and thus the structural vibrational behavior. The wavelength of the standing wave is therefore a crucial factor in detecting crack. A small crack can easily be neglected by a standing wave with long wavelength. Wave of very short wavelength (induced by high frequency), on the other hand, could interact with the micro-crack more effectively.

However, it should be noted that it is not sensible to increase the frequency range indefinitely to achieve higher sensitivity because various external factors would reduce the practicality of the method. For instance, resonance peaks above 200 kHz becomes very closely spaced, rendering the quantification process extremely tedious, if not impossible. Although statistical method could be adopted, physical insight would be sacrificed. Furthermore, the effects of bonding layer and temperature could be very disturbing in such high-frequency range [31,32]. Thus, it is recommended that the frequency range be limited to 200 kHz for practical application. It is also worth mentioning that the sensitivity of EMI technique as shown in Fig. 7 is conceived to be a general observation which could be subjected to changes when the size of structure, type of structure and size of PZT patch are altered.

5.4. Monitoring Crack Propagation Process (Phase II)

The effectiveness of EMI technique in monitoring crack propagation process (phase II) has been studied by Lim and Soh [1], and a semi-analytical damage prognosis suitable for beam structure has also been proposed. The semi-analytical model incorporates both the finite element simulated EMI technique in monitoring a propagating crack and the theory of linear elastic fracture mechanics (Eq. 2) to estimate the remaining useful life of beam structures.

For the sake of completeness, selected results from the abovementioned paper are presented. Figure 8 compares prediction using the semi-analytical model with results of the experimental tests, and illustrates the relationship between reduction in resonance frequency (for a resonance peak at 42.2 kHz) and number of loading cycles. Relatively close agreement between the semi-analytical damage model's prediction and experimental results can be observed. Kindly refer to the abovementioned paper for the development of the model.

The proof-of-concept semi-analytical damage model presented above could provide useful information for monitoring the fatigue crack length and estimating its remaining life. It could serve as an alternative to experimentation to acquire baseline data for damage detection and damage prognosis, especially in the crack propagation stage. However, the characterization of crack initiation process is implicitly considered, and there is also no clear guideline for identifying the critical crack. Both issues are addressed in this paper.

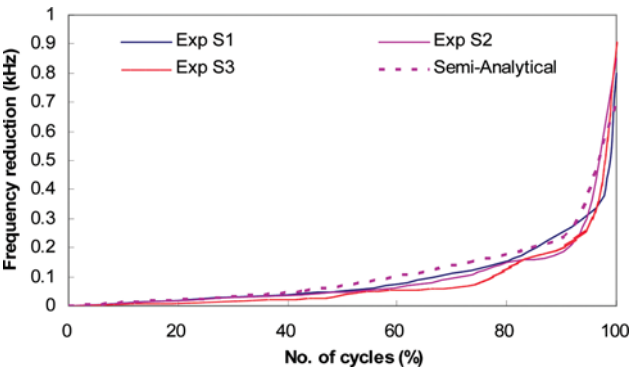

FIGURE 8. Relationship between reductions in resonance frequency (peak at 42.2 kHz) against number of loading cycles obtained from experiment and semi-analytical damage model.

5.5. Critical Crack Identification (Phase III)

One of the most crucial stages of fatigue damage is the third phase—the occurrence of critical crack. At this stage, the structure concerned could only sustain very limited number of cycles before failure. Therefore, a health monitoring technique capable of identifying the critical stage is highly desirable.

In this section, an EMI-based, proof-of-concept qualitative method useful for critical crack identification is proposed. This method requires the visual examination over a range of frequency, which can be expediently explained using Fig. 9. One simply needs to observe the changes in a frequency spectrum as the number of loading cycles increases or as the crack length increases.

We shall first examine Figs. 9(a) and 9(b). In this case, the outlook of the frequency spectrum remains generally the same in comparison to the healthy stage when the number of cycles is less than 190,000, with a 5 mm crack. Movement of peaks is generally small. Almost all peaks shifted slightly to the left without disappearing. Only a few minor peaks

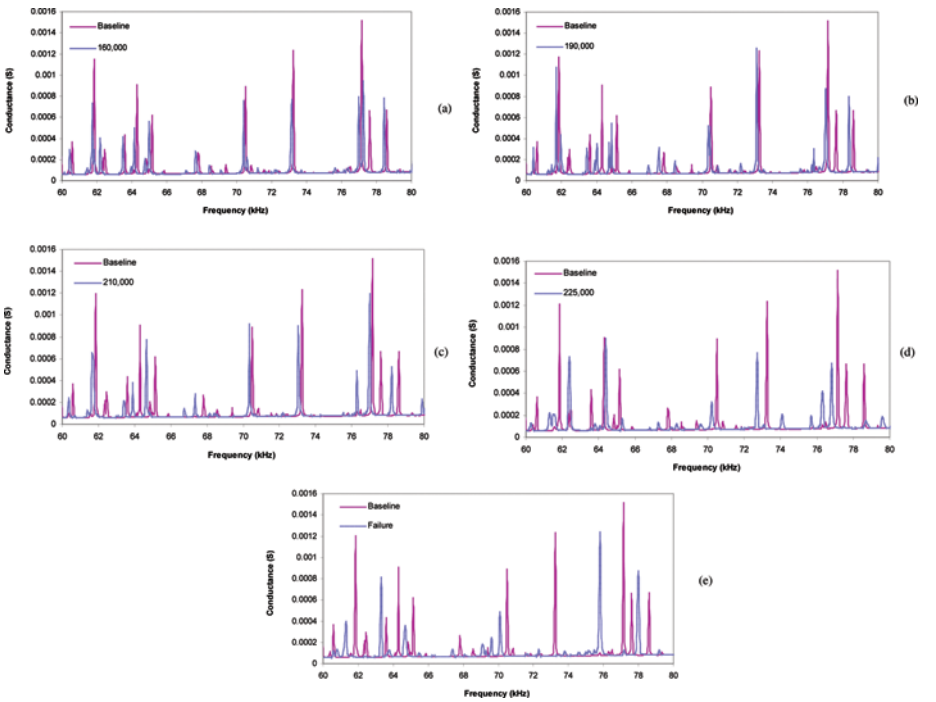

FIGURE 9. Comparison of conductance signatures at various stages of cyclic loading acquired from PZT patch surface bonded on specimen S2 in the frequency range 60 ~ 80 kHz. (a) 160,000 cycles; (b) 190,000 cycles; (c) 210,000 cycles; (d) 225,000 cycles; (e) Failure.

disappeared and a few new minor peaks emerged in Fig. 9(b). After reaching 210,000 cycles, with 9 mm crack (Fig. 9(c)), one major and a few minor peaks at healthy stage disappeared. The frequency spectrum remains similar to the baseline.

After 225,000 cycles, where the critical crack occurred (Fig. 9(d)), the appearance of the frequency spectrum is very different from the baseline. At this stage, identification of original peaks is extremely difficult as some existing major peaks disappeared and some new major peaks emerged, thus changing the outlook of the entire spectrum. At failure point, when the host structure is torn apart (Fig. 9(e)), the frequency spectrum is again totally different from its healthy counterpart. Thus, an inspection of the frequency spectrum can provide a quick way of identifying the status of fatigue cracks.

The abrupt changes in outlook of the frequency spectrum at critical crack length (Fig. 9(d)) can be described as a fundamental change in the vibrational behavior of the host structure. This phenomenon can be physically explained by the fact that the resonance frequencies in the admittance signature spectrum represent the modes of vibration of the host structure. The presence of a relatively small crack would slightly reduce the stiffness of the structure but may not be significant enough to alter its vibrational behavior. As the crack length increases, its effect on the modes of vibration of the beam becomes more impactful, to a point (critical crack)

TABLE 2 Summarized guidelines for qualitative identification of critical crack

Number of cycles (1,000)	Crack length (mm)	Status of crack	Visual appearance of spectrum when compared to healthy stage	Descriptions on peaks' movements
160	1	First crack	Intact	All peaks move slightly to left
190	5	Crack propagation	Largely intact	All peaks move further to left. Some minor peaks disappear while some emerge
210	9	Crack propagation	Similar to healthy stage	Some major peaks cannot be identified. More serious alteration on minor peaks
225	17	Critical crack	Very different from healthy stage	Random peaks' movement. Almost all major and minor peaks cannot be identified
Failure	–	–	Very different from healthy stage	Random peaks' movement. Almost all major and minor peaks cannot be identified

where it alters the major modes of vibration, which can be reflected by the emergence of new resonance peaks or disappearance of the existing resonance peaks.

Generically, the abovementioned qualitative method can be summarized in table form for ease of application, such as the one presented in Table 2. Such table could serve as a useful and handy guideline for critical crack identification by visually inspecting the frequency spectrum. For structure of different sizes, materials, and loadings, the table as well as the frequency range adopted can be modified accordingly. For this method, adoption of moderate frequency range is recommended (40–80 kHz).

6. CONCLUSIONS

This paper presents a series of lab-scale experimental tests to investigate the feasibility of fatigue crack detection and characterization employing the EMI technique. This study extends the study by Lim and Soh [1] by incorporating further studies in the phases involving crack initiation and critical crack.

This study shows that the EMI technique is effective in detecting fatigue induced cracking, even in its incipient stage, or in other words micro-crack. Peaks from higher frequency range (100–200 kHz) are recommended for characterizing micro-crack due to its higher sensitivity. On the other hand, a handy qualitative-based critical crack identification method by visually inspecting the admittance frequency spectrum is suggested.

The semi-analytical damage prognosis model proposed in the previous paper remains useful for fatigue life estimation but is further strengthened by method and recommendations proposed in this paper. At this stage, the technique is proven workable for simple, lab-sized structures, but extension to real-life structures or structural components requires further study.

REFERENCES

1. Y. Y. Lim, and C. K. Soh. *Smart Materials and Structures* **20**:125001 (2011).
2. H. O. Fuchs, and R. I. Stephen. Wiley, New York (1980).
3. L. Pook. Springer, Netherlands (2007).
4. G. Park, H. Sohn, C. R. Farrar, and D. J. Inman. *The Shock and Vibration Digest* **35**:451–463 (2003).
5. F. Dell'Isola, C. Maurini, and M. Porfiri. *Smart Materials and Structures* **13**:299–308 (2004).
6. I. Giorgio, A. Culla, and D. Del Vescovo. *Archive of Applied Mechanics* **79**:859–879 (2009).
7. L. Tang, Y. Yang, and C. K. Soh. *J. Int. Mat. Syst. Struct.* **21**:1867–1897 (2010).
8. F. P. Sun, Z. Chaudhry, C. A. Rogers, M. Majmunder, and C. Liang. *Proceedings of SPIE Conference on Smart Structures and Materials* (I. Chopra ed.), pp. 236–247 February 27, (1995). **2443**, San Diego, California.
9. V. Giurgiutiu, and A. N. Zagrai. *J. Int. Mat. Syst. Struct.* **11**:959–976 (2000).

10. A. S. K. Naidu, and S. Bhalla. *Proceedings of ISSS-SPIE on Smart Materials, Structures and Systems*, Bangalore, India, 639–545 (2002).
11. V. Giurgiutiu. 1st edition, Academic Press, Oxford (2007).
12. Y. Y. Lim, S. Bhalla, and C. K. Soh. *Smart Mat. Struct.* **15**:987–995 (2006).
13. S. Park, J. J. Lee, D. J. Inman, and C. B. Yun. *J. Int. Mat. Syst. Struct.* **19**:509–520 (2008).
14. Y. Y. Lim and C. K. Soh. *J. Int. Mat. Syst. Struct.* **23**:815–826 (2012).
15. Y. Y. Lim, and C. K. Soh. *Smart Struct. Syst.* **11**:349–364 (2013).
16. S. W. Shin, A. R. Qureshi, J. Y. Lee, and C. B. Yun. *Smart Mat. Struct.* **17**:055002 (2008).
17. Y. Yang, B. S. Divsholi, and C. K. Soh. *Sensors* **10**:5193–5208 (2010).
18. S. Park, C. B. Yun, and D. J. Inman. *Fat. Fract. Eng. Mat. Struct.* **31**:714–724 (2008).
19. V. G. M. Annamdas, and C. K. Soh. *J. Int. Mat. Syst. Struct.* **21**:41–59 (2010).
20. V. Giurgiutiu, A. Reynolds, and C. A. Rogers. *J. Int. Mat. Syst. Struct.* **11**:802–812 (1999).
21. V. Giurgiutiu, B. Xu, Y. Chao, S. Liu, and R. Gaddam. *Smart Struct. Syst.* **2**:101–113 (2006).
22. I. Sevostianov, A. Zagrai, A. W. Kruse, and H. C. Hardee. *Int. J. Fract.* **164**:159–166 (2010).
23. M. H. Kim. *J. Int. Mat. Syst. Struct.* **17**:35–44 (2006).
24. J. Ihn, and F. K. Chang. *Smart Mat. Struct.* **13**:609–620 (2004).
25. J. Ihn, and F. K. Chang. *Smart Mat. Struct.* **13**:621–630 (2004).
26. C. K. Soh, and Y. Y. Lim. Advanced Mat. Research **79–82**:2031–2034 (2009).
27. V. G. M. Annamdas. *Inter. J. Aero. Sciences* **1**:8–15 (2012).
28. J. Li, Z. Luo, L. Lin, X. Li, and M. Lei. *Insight-Non-Destructive Testing and Condition Monitoring* **54**:267–271 (2012).
29. R. I. Stephens, A. Fatemi, R. R. Stephens, and H. O. Fuchs. 2nd ed., Wiley, New York (2001).
30. P. I. Ceramic. Piezoelectric ceramic products – fundamentals, characteristics and applications. Lindenstrabe, Germany. Available at: http://www.piceramic.de. (2011).
31. Y. Yang, Y. Y. Lim, and C. K. Soh. *Smart Materials and Structures* **17**:035008 (2008).
32. Y. Yang, Y. Y. Lim, and C. K. Soh. *Smart Mat. Struct.* **17**:035009 (2008).